Limit on the Fierz Interference Term b from a Measurement of the Beta Asymmetry in Neutron Decay

H. Saul,[1] C. Roick,[1] H. Abele,[1,2,3] H. Mest,[3] M. Klopf,[2] A. K. Petukhov,[4] T. Soldner,[4] X. Wang,[1,2] D. Werder,[3] and B. Märkisch[1,3,*]

[1]Physik-Department ENE, Technische Universität München, James-Franck-Straße 1, 85748 Garching, Germany
[2]Technische Universität Wien, Atominstitut, Stadionallee 2, 1020 Wien, Austria
[3]Physikalisches Institut, Universität Heidelberg, Im Neuenheimer Feld 226, 69120 Heidelberg, Germany
[4]Institut Laue-Langevin, 71 avenue des Martyrs, CS 20156, 38042 Grenoble Cedex 9, France

(Received 6 November 2019; accepted 22 July 2020; published 9 September 2020)

In the standard model of particle physics, the weak interaction is described by vector and axial-vector couplings only. Nonzero scalar or tensor interactions would imply an additional contribution to the differential decay rate of the neutron, the Fierz interference term. We derive a limit on this hypothetical term from a measurement using spin-polarized neutrons. This method is statistically less sensitive than the determination from the spectral shape but features much cleaner systematics. We obtain a limit of $b = 0.017(21)$ at 68.27% C.L., improving the previous best limit from neutron decay by a factor of four.

DOI: 10.1103/PhysRevLett.125.112501

Precision measurements of β decays play an important role in understanding the nature of weak interaction and the standard model of particle physics. Neutron beta decay provides a set of observables, including the lifetime τ_n, decay spectra, and angular correlations. These are used to determine couplings and the Cabibbo-Kobayashi-Maskawa matrix element V_{ud} within the standard model, as well as to perform searches for novel scalar and tensor couplings. For a beam of polarized neutrons, the differential decay rate is described by [1]

$$\begin{aligned} &\mathrm{d}\Gamma_n(E_e, \Omega_e, \Omega_\nu, \langle \boldsymbol{\sigma}_n \rangle)\, \mathrm{d}E_e \mathrm{d}\Omega_e \mathrm{d}\Omega_\nu \\ &= \frac{G_\mathrm{F}^2 |V_{ud}|^2}{32\pi^5} \rho(E_e)(1+3\lambda^2) \left\{ 1 + a \frac{\boldsymbol{p}_e \cdot \boldsymbol{p}_\nu}{E_e E_\nu} + b \frac{m_e}{E_e} \right. \\ &\left. \quad + \frac{\langle \boldsymbol{\sigma}_n \rangle}{\sigma_n} \left[A \frac{\boldsymbol{p}_e}{E_e} + B \frac{\boldsymbol{p}_\nu}{E_\nu} + D \frac{\boldsymbol{p}_e \times \boldsymbol{p}_\nu}{E_e E_\nu} \right] \right\}, \end{aligned} \tag{1}$$

with momenta of the electron p_e and the neutrino p_ν, their energies E_e and E_ν, the neutron spin $\boldsymbol{\sigma}_n$, the phase space density $\rho(E_e)$, and the decay parameters a, b, A, B, and D. Within the standard model, the correlation coefficients a, A, and B depend solely on the ratio of axial-vector and vector coupling constants, $\lambda = g_\mathrm{A}/g_\mathrm{V}$, and the T-violating parameter D is related to the phase of λ. The beta asymmetry parameter A quantifies the parity-violating beta asymmetry and is most sensitive to $|\lambda|$. Neglecting order 1% corrections and assuming λ real, the asymmetry A is given by [2]

$$A_0 = -2 \frac{\lambda(\lambda+1)}{1+3\lambda^2}. \tag{2}$$

A has been measured with high accuracy in [3–5].

The shape of the electron spectrum given by the phase space density is independent of whether the weak interaction is generated by vector and axial-vector couplings $(V-A)$ or scalar and tensor couplings $(S-T)$ [6]. However, in case of hypothetical scalar or tensor couplings in addition to the $V-A$ interaction of the standard model, the beta spectrum would be modified by the Fierz interference term b as follows:

$$b \simeq \frac{g_S g_V + 3 g_A g_T}{g_V^2 + g_S^2 + 3(g_A^2 + g_T^2)} \simeq 2 \frac{g_S + 3\lambda g_T}{1+3\lambda^2}, \tag{3}$$

with coupling constants $g_{V,A,S,T}$. Such a contribution would change the overall decay probability of unpolarized neutrons according to Eq. (1) and also change the measured values $\tilde{X}$ of many of the correlation coefficients X (see also Refs. [7,8]) as follows:

$$\tilde{X} = X \cdot \left(1 + \left\langle b \frac{m_e}{E_e} \right\rangle \right)^{-1}. \tag{4}$$

Combining several measured correlation coefficients allows one to simultaneously determine λ and place limits on scalar and tensor couplings. Alternatively, limits on left-handed tensor interactions can also be obtained by combining the measured beta asymmetry parameter with the stringent limits on scalar interactions from superallowed beta decays [9], see Refs. [5,10]. For recent reviews, surveys, and limits on couplings beyond the standard model, see Refs. [8,11–19]. A large Fierz term of $O(10^{-2})$ would be required by the proposed dark decay to explain discrepancies in neutron lifetime measurements using different methods [20].

In order to put a *direct* constraint on the Fierz interference term b from a single measurement, either the spectral shape of the beta spectrum from unpolarized neutrons or the asymmetry spectrum corresponding to one of the correlation coefficients needs to be analyzed. A first analysis of the unpolarized beta spectrum has been published in [21]. Currently, this type of analysis is clearly limited by detector systematics. However, the same principle will be utilized with upcoming measurements to be performed by Nab [22–24], NOMOS [25,26], and PERC [27–29].

In this Letter, we present for the first time an analysis of the experimental beta asymmetry spectrum to derive a limit on the Fierz interference term. While this method provides a smaller statistical sensitivity reduced by about an order of magnitude compared to a limit from the beta spectrum directly [30], detector and background systematics are strongly suppressed. This leads to an improved limit on the Fierz term derived from the largest available dataset in neutron beta decay obtained by the instrument PERKEO III of 6×10^8 decay events. The result is purely limited by statistics.

The analysis presented herein extends the results of [5] to a correlated analysis in A and b. For a description of the experimental setup, see [5,31,32], which include a schematic of the spectrometer.

PERKEO III was installed at the PF1B cold neutron beam facility at the Institut Laue-Langevin, which offers a neutron capture flux density of $\Phi = 2 \times 10^{10}\ \mathrm{s^{-1}\,cm^{-2}}$ [33]. The neutron beam is limited in wavelength to 5 Å with about 10% FWHM by means of a Dornier velocity selector. A bender type supermirror polarizer [34] is used to select neutrons with a certain spin direction that can be reversed with an adiabatic fast passage spin flipper [35]. After the flipper, the neutron beam passes a collimation system consisting of five ^{6}LiF apertures, which limit the cross section and divergence of the neutron beam. A rotating disc chopper is mounted directly in front of the spectrometer to create a pulsed neutron beam [31]. During the measurement, two different chopper frequencies (94 and 83 Hz) have been used.

The core component of the spectrometer is an 8 m long, normal conducting magnet system that surrounds the vacuum vessel. The central part of the spectrometer features a nearly homogeneous magnetic field with a maximum of $B_{\mathrm{max}} = 152.7$ mT and a length of 2.7 m. This part acts as the central decay volume in which the charged decay particles from neutron decay are collected by the magnetic field. The charged decay particles are separated from the neutron beam by curved magnetic field sections and are guided to the two detectors. The remaining neutron beam is dumped into a $^{10}B_4C$ beam stop.

The electron detectors consist of Bicron BC-400 plastic scintillators, each read out on two sides by a total of six fine-mesh photomultipliers of type Hamamatsu R5504/R5924. The photomultipliers are connected to the scintillator via acrylic light guides. The scintillators have a thickness of 5 mm, which allows full energy deposition of electrons up to an energy of 1.0 MeV at normal incidence and minimum sensitivity to γ rays. The active area of the detectors is $43 \times 45\ \mathrm{cm^2}$.

In order to monitor and calibrate the detectors, multiple electron conversion sources (^{139}Ce, ^{113}Sn, ^{137}Cs, ^{207}Bi) are installed inside the decay volume of PERKEO III. These provide five calibration peaks covering an energy range from 0.1 to 1 MeV. The sources are deposited on ultrathin carbon foils with a thickness of about 100 nm. They are mounted on a mechanical apparatus in the central volume, allowing one to move the sources in two dimensions to measure the detector responses and to map out their uniformity.

The data used in this analysis is a subset of the data used in Ref. [5]. It consists of four datasets, each representing one chopper frequency and the detector that triggered first. About 20% of the data have been excluded due to missing corresponding measurements of the detector uniformity. These data are needed to calculate potentially substantial systematic corrections to this correlated analysis with a potentially large impact on the analysis of b. In total, about 4.8×10^8 decay events are included in the analysis.

Neglecting quadratic contributions of scalar and tensor interactions to the beta asymmetry parameter A, the basic expression that is used in this analysis is the experimental asymmetry spectrum

$$A_{\mathrm{exp}}(E_e) = \frac{N^{\uparrow}(E_e) - N^{\downarrow}(E_e)}{N^{\uparrow}(E_e) + N^{\downarrow}(E_e)} = \frac{v(E_e) A(\lambda) P_n M}{2c(1 + b\frac{m_e}{E_e})}, \quad (5)$$

with λ and b as free parameters and with the electron velocity $v(E_e)$, the average neutron beam polarization $\mathbf{P}_n = \langle \boldsymbol{\sigma}_n \rangle / \sigma_n$, and the correction M to account for the magnetic mirror effect due to the shape of the magnetic field (see below). The arrows $\uparrow\downarrow$ indicate the neutron spin direction. The factor $1/2$ stems from the integration of the angular cosine distribution. The full fit function contains theoretical corrections to account for proton recoil, weak magnetism, and radiative corrections [2,36]. These are functions of λ and the electron energy E_e. In order to facilitate comparison and use in new physics searches, we provide results in terms of $A(\lambda)$ instead of λ.

The factors P_n and M represent the dominant experimental corrections to the measurement of the beta asymmetry and have been analyzed separately in order to ensure a *blinded* analysis [5]. They scale the amplitude of the experimental beta asymmetry and thus the result for A, whereas b is only affected due to the corresponding change in the theoretical corrections and correlations between the parameters.

On top of the underlying fit function, a semianalytical model of the detector response is applied to account for

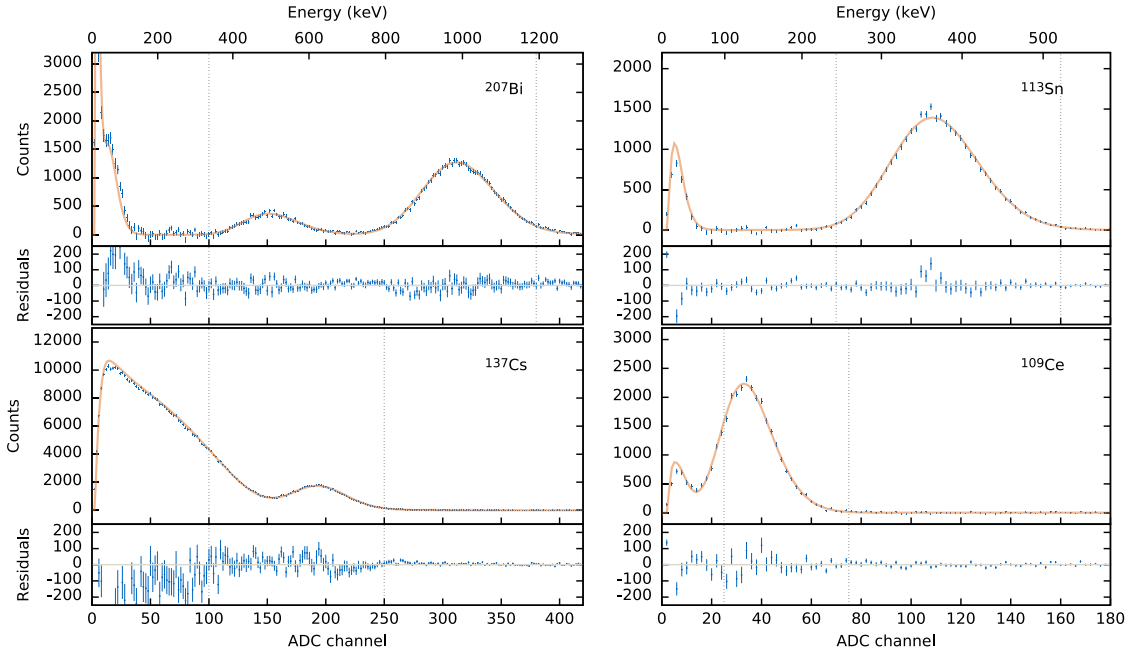

FIG. 1. Example of measured calibration spectra and the simultaneous fit performed to extract the free parameters of the detector response model. The dashed vertical lines indicate the fit regions. The spectra are practically free of γ background from the sources. The discrepancies at low energy outside the fit range mostly stem from uncertainties in the exact shape of the trigger function. We only show every other data point to improve the presentation.

relevant effects. These include nonlinearity effects in the scintillator and electronics, broadening of the signal due to photoelectron conversion inside the photomultipliers, and the photomultiplier gain process and electronic noise in the data acquisition system, as well as the mapping of the signal amplitude to channels of the analog-to-digital converter.

The free parameters of the detector response model are determined using a simultaneous fit to measured calibration spectra. The quality of the fits can be seen in Fig. 1 for one out of 114 calibration sets obtained within the 60 days of measurement. The plastic scintillators of PERKEO III have a low sensitivity for γ radiation, and the solid angle for γ radiation from the sources onto the detectors is negligibly small.

Leading systematic effects are related to the detector response: the nonlinear detector response function, temperature stability, uniformity, and electron backscattering. The resulting corrections and uncertainties are uncorrelated and small compared to the statistical uncertainties. This allows for separate treatment of the individual systematic effects. The corresponding uncertainties are extracted as a covariance matrix that is diagonal with respect to the dominant systematic shift observed in A and b. This allows one to also account for the correlation induced by systematic effects. The different relevant systematic effects are discussed below; the respective corrections and uncertainties are summarized in Table I.

Nonlinearity.—The response of the detectors is not linear with respect to the energy of the detected electrons. One

TABLE I. Summary of corrections and uncertainties (in parentheses) to A and b. In contrast to Ref. [5], we provide the magnitude of the corrections, not fractional ones. Corrections that contribute only on the 10^{-5} level are omitted. One of the fit parameters is actually λ, not A, but we list corrections on A for comparability with earlier measurements.

	Correction	
Effect on $\boldsymbol{A}$ and $\boldsymbol{b}$	on $\boldsymbol{A}$ (10^{-4})	on $\boldsymbol{b}$ (10^{-3})
Neutron beam		
Polarization and Spin-flip efficiency	−11.4(0.9) [a]	0.5(0.6) [a]
Background		
Time variation	0.02(0.12)	0.04(0.24)
Chopper	0.09(0.22)	0.5(0.4)
Electrons		
Magnetic mirror effect	0 − 6.4(0.6) [a]	1.0(0.4) [a]
Undetected backscattering	3.7(1.1)	−6.4(1.9)
Electron detector		
Temporal stability	(0.6) [a]	(1.2) [a]
Nonuniformity	0.6(0.7)	−1.1(1.3)
Nonlinearity	0.8(1.0)	−0.8(1.6)
Theory		
Radiative corrections	−1.0(0.3) [a]	3.5(0.5) [a]
Total systematics	−12.8(2.1)	−6.1(3.2)
Statistical uncertainty	(14.4)	(20.4)
Total	(14.6)	(20.6)

[a]Already included in the fit shown in Fig. 2; measured by the data acquisition system or included in the fit function.

contribution to the nonlinearity is caused by saturation effects in the light generation inside the scintillator, which is empirically described by the Birks model [37] using the quenching parameter k_B. Recent measurements for similar scintillator materials yield $k_B = 100$–150 nm/keV [38], which we confirmed for our scintillator by independent test measurements using Compton recoil electrons from γ radiation [39]. Another contribution to the nonlinearity arises from bandwidth limitations in the electronics used. Although studied in off-line measurements, the determination of the exact contribution of the electronics to the detector nonlinearity would require a full reproduction of the original detector setup. Instead, the analysis is done with three different models to describe the overall nonlinearity of the detector response and with and without the calibration point at 1 MeV. The free parameters of these models are obtained from fits to spectra from calibration sources. A pure Birks model to describe the combined nonlinearity of scintillator and electronics leads to $k_B \simeq 400$ nm/keV dependent on the dataset. The maximum difference between the results of the three methods is taken as systematic uncertainty.

Stability.—The gain of the detector varies over time, mainly due to fluctuations in the temperature. This effect can be as large as 2% between day and night. The detector gain has been monitored hourly using a single calibration source, and the signal amplitudes have been renormalized in the data reduction process by interpolating between these hourly measurements. With this method, the detector gain is effectively stabilized on the 10^{-3} level. However, the remaining fluctuations still contribute one of the dominant systematic uncertainties related to the detector response.

Detector Uniformity.—The detector response varies spatially due to the variation in photon transport efficiency inside the scintillator. This leads to a relative deviation from uniformity by less than $\pm 2.5\%$ over the area covered by decay electrons. The spatial response of the detectors was mapped weekly using a single calibration source at different positions. The difference in detector coverage between calibration measurements and measurements of the beta asymmetry leads to a small change in the effective signal response for the two types of measurements. This includes the dependence of the magnetic point spread of electrons on the beta asymmetry itself [40,41]. In order to account for these differences, the corresponding spectral corrections are calculated using photon transport simulations performed with GEANT4 [42], which are matched to the measured spatial detector response. The consistent characterization of the detector without resorting to beta decay data is a major improvement of this measurement.

Undetected Backscattering.—The symmetric design of PERKEO III with two detectors connected by the magnetic field enables reconstruction of the full electron energy even if electrons are backscattered from the scintillator, as both detectors are always read out simultaneously. This backscattering occurs with a probability of about 11% [43] and is suppressed by reflections at the magnetic field to 6% of events where the electron reaches the opposite detector (see also [44]). Because of the finite trigger threshold with an efficiency of 50% at channel ≈5.5 (corresponding to ≈30 keV), the energy deposited in the first detector in rare cases is not sufficient to trigger the electronics, and the wrong emission direction and energy are assigned to the event. This changes the asymmetry and the shape of the measured asymmetries $A_{\mathrm{exp}}(E_e)$ for both detectors. An energy-dependent correction for undetected backscattering is included in the analysis, which is calculated based on backscattering simulations performed with GEANT4 [42] and verified against measured data. Details on undetected backscattering in PERKEO III can be found in [43].

Background.—The pulsed beam allows one to select events according to their neutron time of flight from the chopper within the spectrometer. The time window is chosen such that the neutron pulse is fully contained in the central decay volume, without any contact to material, and all decay electrons are guided to one of the detectors. After the neutron pulse is absorbed by the beamstop, another time window is used to extract the background. This way signal and background are measured during every chopper cycle with the chopper being closed. In addition to the electron detectors, NaI γ detectors have been used to investigate the time dependence of the ambient background and that created by the chopper disc. Both effects have been found to be on the 10^{-5} and 10^{-4} level for A and b, respectively. The effect of the background subtraction can be seen in Fig. 2 of Ref. [5]. In Table I, we separately list contributions by the (non)uniformity of the chopper disc

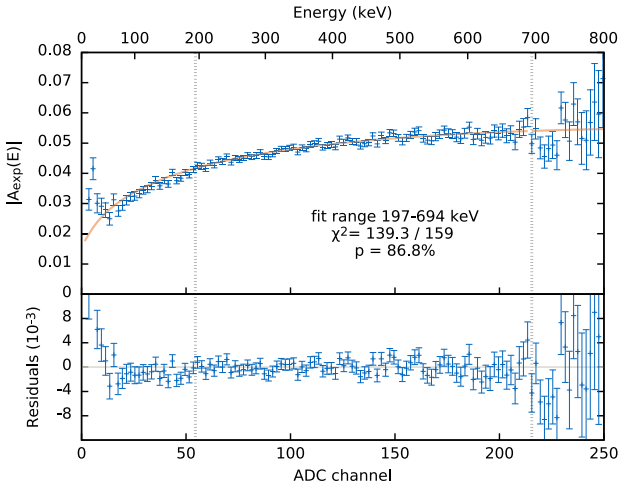

FIG. 2. Fit to the data at the chopper frequency of 83 Hz measured by the downstream detector. The fit includes theoretical corrections as well as the full model of the detector response. Corrections for detector nonuniformity and undetected backscattering are not included. The data is rebinned by a factor of 2 for presentation. The fit range is indicated by the dashed vertical lines.

and potential variation in time within the background time window.

Figure 2 shows a fit to one of the four datasets. As was the case already with the single parameter fits in Ref. [5], the fit quality is excellent for all individual datasets. The energy range of the fit was extended to 197–694 keV compared to [5] to optimize the total error of this two-parameter fit (λ and b). The results of all datasets are consistent with statistical fluctuations. We obtain a combined result of

$$\begin{aligned} A &= -0.1209(14)_{\mathrm{stat}}(2)_{\mathrm{sys}} = -0.1209(15), \\ b &= 0.017(20)_{\mathrm{stat}}(3)_{\mathrm{sys}} = 0.017(21), \\ \rho_{A,b} &= -0.985, \end{aligned} \tag{6}$$

with one sigma errors ($\Delta\chi^2 = 1$) and where $\rho_{A,b}$ is the off-diagonal element of the correlation matrix. The fit result for λ corresponding to A is $\lambda = -1.2792(60)$. This result includes the systematic corrections that are summarized in Table I and the propagated statistical uncertainties of the free parameters of the detector response model as obtained from the calibration analysis. However, these contributions on the 10^{-5} and 10^{-4} level for A and b, respectively, are negligible. Figure 3 compares the error ellipses resulting from statistical and systematic uncertainties, where statistical uncertainties are dominating.

Assuming the standard model with $b \equiv 0$, we obtain from our correlated result in Eq. (6)

$$A = -0.11972(25), \qquad \lambda = -1.27607(68), \tag{7}$$

in agreement with our analysis within the standard model in Ref. [5], which we recommend if scalar and tensor interactions are assumed to be absent. The 90% confidence region corresponding to the Fierz result in Eq. (6) is

$$-0.018 \leq b \leq 0.052. \tag{8}$$

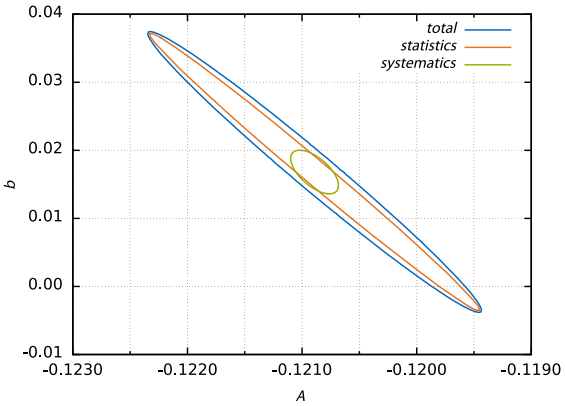

FIG. 3. 68.27% confidence region for the beta asymmetry parameter A and Fierz interference parameter b and the contributions by statistics and systematics.

To date this is the most precise limit on b obtained from a single measurement in neutron decay.

In conclusion, we have demonstrated the extraction of limits on the Fierz interference term from a measurement of beta asymmetry spectra in *polarized* neutron decay. In contrast to a more direct determination from the spectrum in *unpolarized* neutron decay, this method profits from much better controlled systematics and is limited by available statistics. Next generation instruments like PERC [27,28] will allow the measurement of decay correlations with strongly improved statistical uncertainties. The correlated analysis of A and b in these measurements will become even more important and serve as valuable input to derive limits on scalar and tensor couplings from beta decay data [8].

The authors acknowledge the excellent support of the services of the Physikalisches Institut, Heidelberg University, and the ILL. We thank D. Rechten, TUM, for providing us with ultrathin carbon foils, and U. Schmidt, Heidelberg, and M. González-Alonso, València, for valuable discussions. We thank D. Dubbers for his support and enthusiasm. This work was supported by the Priority Programme SPP 1491 of the German Research Foundation, Contracts No. MA 4944/1-2, No. AB 128/5-2, and No. SO 1058/1-1; the Austrian Science Fund, Contracts No. P 26636-N20 and No. W1252-N27 (DK-PI); the German Federal Ministry for Research and Education, Contracts No. 06HD153I and No. 06HD187; and the DFG cluster of excellence "Origin and Structure of the Universe." The computational results presented have been achieved in part using the Vienna Scientific Cluster.

Note added.—Meanwhile, Ref. [45] presents a similar analysis by the UCNA collaboration and extends the analysis of the beta spectrum from unpolarized neutron decay of [21].

*Corresponding author.
maerkisch@ph.tum.de

[1] J. D. Jackson, S. B. Treiman, and H. W. Wyld, Possible tests of time reversal invariance in beta decay, Phys. Rev. **106**, 517 (1957).
[2] D. Wilkinson, Analysis of neutron β-decay, Nucl. Phys. **A377**, 474 (1982).
[3] D. Mund, B. Märkisch, M. Deissenroth, J. Krempel, M. Schumann, H. Abele, A. Petoukhov, and T. Soldner, Determination of the Weak Axial Vector Coupling $\lambda = g_A/g_V$ from a Measurement of the β-Asymmetry Parameter A in Neutron Beta Decay, Phys. Rev. Lett. **110**, 172502 (2013).
[4] M. A.-P. Brown *et al.* (UCNA Collaboration), New result for the neutron β-asymmetry parameter A_0 from UCNA, Phys. Rev. C **97**, 035505 (2018).
[5] B. Märkisch, H. Mest, H. Saul, X. Wang, H. Abele, D. Dubbers, M. Klopf, A. Petoukhov, C. Roick, T. Soldner,

and D. Werder, Measurement of the Weak Axial-Vector Coupling Constant in the Decay of Free Neutrons Using a Pulsed Cold Neutron Beam, Phys. Rev. Lett. **122**, 242501 (2019).

[6] T. D. Lee and C. N. Yang, Question of parity conservation in weak interactions, Phys. Rev. **104**, 254 (1956).

[7] M. González-Alonso and O. Naviliat-Cuncic, Kinematic sensitivity to the Fierz term of β-decay differential spectra, Phys. Rev. C **94**, 035503 (2016).

[8] M. González-Alonso, O. Naviliat-Cuncic, and N. Severijns, New physics searches in nuclear and neutron β decay, Prog. Part. Nucl. Phys. **104**, 165 (2019).

[9] J. C. Hardy and I. S. Towner, Superallowed $0^+ \to 0^+$ nuclear β decays: 2014 critical survey, with precise results for V_{ud} and CKM unitarity, Phys. Rev. C **91**, 025501 (2015).

[10] R. W. Pattie, K. P. Hickerson, and A. R. Young, Limits on tensor coupling from neutron β-decay, Phys. Rev. C **88**, 048501 (2013); Erratum, Phys. Rev. C **92**, 069902 (2015).

[11] C. C. Chang, A. N. Nicholson, E. Rinaldi, E. Berkowitz, N. Garron, D. A. Brantley, H. Monge-Camacho, C. J. Monahan, C. Bouchard, M. A. Clark, B. Joó, T. Kurth, K. Orginos, P. Vranas, and A. Walker-Loud, A per-cent-level determination of the nucleon axial coupling from quantum chromodynamics, Nature (London) **558**, 91 (2018).

[12] L. Hayen and N. Severijns, Radiative corrections to Gamow-Teller decays, arXiv:1906.09870.

[13] B. R. Holstein, Precision frontier in semileptonic weak interactions: Theory, J. Phys. G **41**, 114001 (2014), Focus Section.

[14] F. Wauters, A. García, and R. Hong, Limits on tensor-type weak currents from nuclear and neutron β decays, Phys. Rev. C **89**, 025501 (2014).

[15] V. Cirigliano, S. Gardner, and B. R. Holstein, Beta decays and non-standard interactions in the LHC era, Prog. Part. Nucl. Phys. **71**, 93 (2013).

[16] T. Bhattacharya, V. Cirigliano, S. D. Cohen, A. Filipuzzi, M. González-Alonso, M. L. Graesser, R. Gupta, and H.-W. Lin, Probing novel scalar and tensor interactions from (ultra)cold neutrons to the LHC, Phys. Rev. D **85**, 054512 (2012).

[17] K. K. Vos, H. W. Wilschut, and R. G. E. Timmermans, Symmetry violations in nuclear and neutron β decay, Rev. Mod. Phys. **87**, 1483 (2015).

[18] D. Dubbers and M. G. Schmidt, The neutron and its role in cosmology and particle physics, Rev. Mod. Phys. **83**, 1111 (2011).

[19] H. Abele, The neutron. Its properties and basic interactions, Prog. Part. Nucl. Phys. **60**, 1 (2008).

[20] A. Ivanov, R. Höllwieser, N. Troitskaya, M. Wellenzohn, and Y. Berdnikov, Neutron dark matter decays and correlation coefficients of neutron β-decays, Nucl. Phys. **B938**, 114 (2019).

[21] K. P. Hickerson *et al.* (UCNA Collaboration), First direct constraints on Fierz interference in free-neutron β decay, Phys. Rev. C **96**, 042501(R) (2017).

[22] D. Počanić *et al.*, Nab: Measurement principles, apparatus and uncertainties, Nucl. Instrum. Methods Phys. Res., Sect. A **611**, 211 (2009).

[23] S. Baeßler, J. D. Bowman, S. Penttilä, and D. Počanić, New precision measurements of free neutron beta decay with cold neutrons, J. Phys. G **41**, 114003 (2014).

[24] J. Fry *et al.*, The Nab experiment: A precision measurement of unpolarized neutron beta decay, EPJ Web Conf. **219**, 04002 (2019).

[25] X. Wang, G. Konrad, and H. Abele, $R \times B$ drift momentum spectrometer with high resolution and large phase space acceptance, Nucl. Instrum. Methods Phys. Res., Sect. A **701**, 254 (2013).

[26] D. Moser, H. Abele, J. Bosina, H. Fillunger, T. Soldner, X. Wang, J. Zmeskal, and G. Konrad, NoMoS: An $R \times B$ drift momentum spectrometer for beta decay studies, EPJ Web Conf. **219**, 04003 (2019).

[27] D. Dubbers, H. Abele, S. Baeßler, B. Märkisch, M. Schumann, T. Soldner, and O. Zimmer, A clean, bright, and versatile source of neutron decay products, Nucl. Instrum. Methods Phys. Res., Sect. A **596**, 238 (2008).

[28] G. Konrad *et al.* (PERC Collaboration), Neutron decay with PERC: A progress report, J. Phys. **340**, 012048 (2012).

[29] X. Wang, C. Ziener *et al.* (PERC Collaboration), Design of the magnet system of the neutron decay facility PERC, EPJ Web Conf. **219**, 04007 (2019).

[30] F. Glück, I. Joó, and J. Last, Measurable parameters of neutron decay, Nucl. Phys. **A593**, 125 (1995).

[31] B. Märkisch, H. Abele, D. Dubbers, F. Friedl, A. Kaplan, H. Mest, M. Schumann, T. Soldner, and D. Wilkin, The new neutron decay spectrometer PERKEO III, Nucl. Instrum. Methods Phys. Res., Sect. A **611**, 216 (2009).

[32] B. Märkisch, Systematic advantages of pulsed beams for measurements of correlation coefficients in neutron decay, Phys. Procedia **51**, 41 (2014).

[33] H. Abele, D. Dubbers, H. Häse, M. Klein, A. Knöpfler, M. Kreuz, T. Lauer, B. Märkisch, D. Mund, V. Nesvizhevsky, A. Petoukhov, C. Schmidt, M. Schumann, and T. Soldner, Characterization of a ballistic supermirror neutron guide, Nucl. Instrum. Methods Phys. Res., Sect. A **562**, 407 (2006).

[34] T. Soldner *et al.*, Installation and first tests of the new PF1b polariser, Institut Laue-Langevin, Grenoble, France, Technical Report ILL03SO10T, 2002.

[35] A. Bazhenov, V. Lobashev, A. Pirozhkov, and V. Slusar, An adiabatic resonance spin-flipper for thermal and cold neutrons, Nucl. Instrum. Methods Phys. Res., Sect. A **332**, 534 (1993).

[36] A. N. Ivanov, M. Pitschmann, and N. I. Troitskaya, Neutron β^- decay as a laboratory for testing the standard model, Phys. Rev. D **88**, 073002 (2013).

[37] J. B. Birks, Scintillations from organic crystals: Specific fluorescence and relative response to different radiations, Proc. Phys. Soc. London Sect. A **64**, 874 (1951).

[38] C. Aberle, C. Buck, F. X. Hartmann, S. Schönert, and S. Wagner, Light output of Double Chooz scintillators for low energy electrons, J. Instrum. **6**, P11006 (2011).

[39] H. Saul, Energy Dependence of the Beta Asymmetry in Neutron Beta Decay, Ph. D. thesis, Technische Universität München and Technische Universität Wien, 2018, http://nbn-resolving.de/urn/resolver.pl?urn:nbn:de:bvb:91-diss-20181127-1459307-1-8.

[40] D. Dubbers, L. Raffelt, B. Märkisch, F. Friedl, and H. Abele, The point spread function of electrons in a magnetic field,

and the decay of the free neutron, Nucl. Instrum. Methods Phys. Res., Sect. A **763**, 112 (2014).
[41] D. Dubbers, Magnetic guidance of charged particles, Phys. Lett. B **748**, 306 (2015).
[42] J. Allison *et al.*, Recent developments in GEANT4, Nucl. Instrum. Methods Phys. Res., Sect. A **835**, 186 (2016).
[43] C. Roick, H. Saul, H. Abele, and B. Märkisch, Undetected electron backscattering in PERKEO III, EPJ Web Conf. **219**, 04005 (2019).
[44] H. Abele, G. Helm, U. Kania, C. Schmidt, J. Last, and D. Dubbers, On the origin of the 17 keV neutrino signals, and a loss-free measurement of the ^{35}S β-spectrum, Phys. Lett. B **316**, 26 (1993).
[45] X. Sun *et al.* (UCNA Collaboration), Improved limits on Fierz interference using asymmetry measurements from the ultracold neutron asymmetry (UCNA) experiment, Phys. Rev. C **101**, 035503 (2020).